Heliyon 6 (2020) e04902

Contents lists available at ScienceDirect

Heliyon

journal homepage: www.cell.com/heliyon

Research article

Thermogravimetric analysis of the combustion of marine microalgae *Spirulina platensis* and its blend with synthetic waste

Sukarni Sukarni [a,b,*]

[a] *Center for Renewable and Sustainable Energy Engineering (CRSEE), Department of Mechanical Engineering, Universitas Negeri Malang, Jl. Semarang No 5, Malang, 65145, Indonesia*

[b] *Centre of Advanced Materials for Renewable Energy, Universitas Negeri Malang, Jl. Semarang No 5, Malang, 65145, Indonesia*

ARTICLE INFO

Keywords:
Energy
Combustion
Kinetic
Fitting model
Spirulina platensis
Synthetic wastes

ABSTRACT

The thermal decomposition of the microalgae *Spirulina platensis,* synthetic wastes, and their blends under an oxidative atmosphere and their kinetic parameters were investigated using a thermogravimetric analyzer. Three stages were observed during the combustion of the blended fuels, and two distinct peaks occurred in the second stage. A kinetic analysis during combustion was studied according to the fitting method proposed by Coats-Redfern and Horowitz-Metzger. The addition of the microalgae to the synthetic waste led to an increase in the apparent activation energies in Zone I in the second stage, whereas an increasing proportion of the microalgae in the blends resulted in decreasing apparent activation energies in Zone II in the second stage.

1. Introduction

Increasing prosperity, living standards, and population mean that worldwide energy demand will increase by around a third by 2040, and India, China, and other Asia are predicted to contribute to two-thirds of the increase [1]. However, fossil-based energy resources are becoming exhausted, and the carbon dioxide which is released during the combustion process has alarming consequences on the environment. To guarantee future survival, developing sufficient supplies of environmentally-friendly and renewable energy is critical [2, 3, 4, 5]. Among renewable energy sources, biomass has emerged as an excellent contender for energy production due to its abundance and the fact that it can be sourced from all over the world. Biomass also naturally reduces carbon dioxide in the environment through photosynthesis.

Feedstocks for bio-energy can be classified into four generations. The first generation is derived from food crops, the second generation originates from lignocellulosic biomass, the third generation is produced from aquatic biomass feedstock, and the fourth generation is generated through metabolically engineering oxygenic photosynthetic microorganisms for biofuel [6]. The main obstacles in the widespread adoption of the first-generation biofuel were due to the dilemma of food versus fuel and problems associated with the competition between arable land and ecosystem balancing [2, 7]. However, various studies have advanced the belief that microalgae may have the potential to replace conventional fuel.

A major obstacle in large-scale microalgae utilization for alternative fuel is the high water content of dilute algae solutions, which results in high operational costs during dewatering. Research indicates that the cost of harvesting is 20–30% of the total cost [8, 9] and the high capital consumption that results from the small size of the cells that dissolve in water, leading to large volumes that must be processed during harvesting and dewatering [8, 10]. If direct combustion is selected as a technique for thermochemical conversion, then it is only feasible with biomass material that has a moisture content of less than 50% [11]. Many researchers have tried to address this inherent drawback [12, 13, 14, 15, 16, 17]. Although water removal from algae biomass is yet to achieve an economically reasonable cost, studying the high-quality and valuable fuels generated from microalgae species is still beneficial.

Spirulina platensis (SP) is a cyanobacterium and a blue-green algae species that grow in brackish or freshwater, as well as in marine environments, located around the tropical zone and equatorial and formed the filaments in the culture medium [18, 19, 20]. In aquaculture, SP is utilized as a feed additive to improve the growth of several fish species [21]. These microalgae have a relatively large size, and can, therefore, be easily and inexpensively collected by filtration from a medium [22]. Using an appropriate lighting method, the biomass of SP can be increased by over 76.72% of its natural growth levels [23]. In Indonesia, this algae

* Corresponding author.
E-mail address: sukarni.ft@um.ac.id.

https://doi.org/10.1016/j.heliyon.2020.e04902
Received 4 November 2018; Received in revised form 2 July 2020; Accepted 7 September 2020

Table 1. The fundamentals properties of SP and SW.

Sample	Proximate analysis (wt,%)				Ultimate analysis (wt,%)					Colorific value (MJ/kg)	Chemical composition (wt, %)		
	M_{adb}	VM_{db}	FC_{db}	A_{db}	C_{db}	H_{db}	O_{db}	N_{db}	S_{db}		$Protein_{daf}$	$Lipid_{daf}$	$Carbohydrate_{daf}$
SP	8.66	77.96	11.90	10.14	51.81	7.11	32.90	3.95	1.27	20.97	65.64	27.17	7.20
SW	0.75	85.91	6.07	8.02	80.77	9.22	1.68	0.24	0.09	31.92	-	-	-

adb: air-dried basis, db: dry basis, daf: dry and ash-free basis.

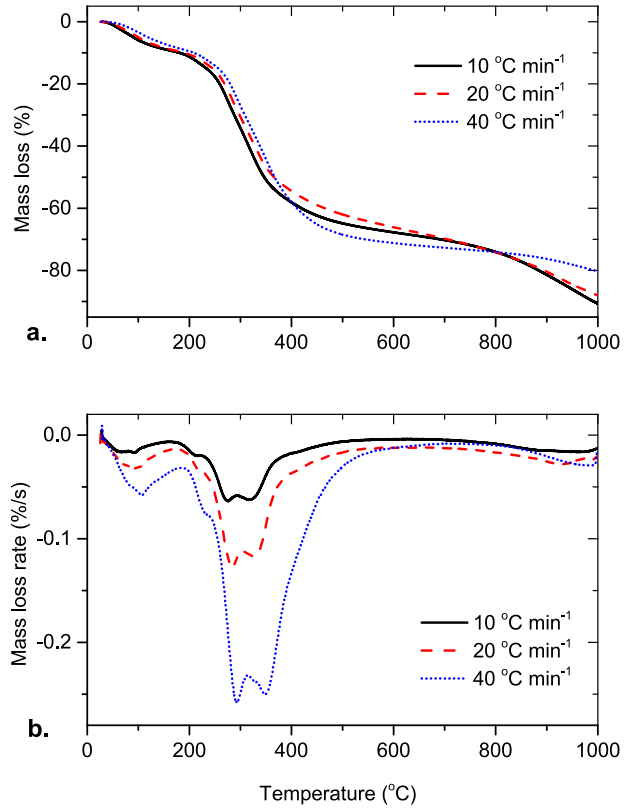

Figure 1. The curves of SP combustion at different heating rates: a. TG curves, b. DTG curves.

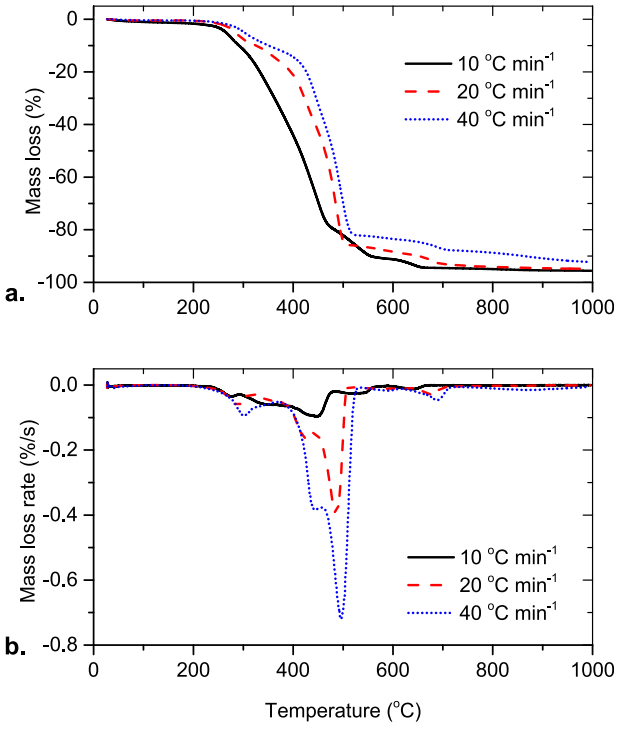

Figure 2. The curves of SW combustion at different heating rates: a. TG curves, b. DTG curves.

species is abundant and widespread and is particularly common in fish hatcheries. Several studies have explored the thermal characteristics of SP in relation to its potential use as a biomass fuel feedstock based on pyrolysis [19, 24] and have studied its combustion characteristics [25]. However, the co-combustion of SP and synthetic waste (SW) has not been investigated in detail.

City developments in Indonesia have led to urban lifestyle changes, and the use of synthetic-based materials in daily life has significantly increased, resulting in substantial SW growth. This waste is non-biodegradable and does not decompose naturally and as such is a significant environmental pollutant. In recent times, 10,660,505 kg/day of SW, particularly plastic, has been generated in Indonesia [26]. The fast growth of SW is a pressing problem as it accumulates in cities and pollutes the ocean. Landfilling, which is currently the main method for disposing of SW, is unsuitable in the long-term as a buildup of SW could interfere with soil fertility and pollute the land, soil, and water. From the literature point of view, the thermal conversion of wastes is the most widely chosen due to its ability to reduce waste volume and its effectiveness in recovering energy.

The utilization of SW for energy generation in Indonesia has not garnered significant attention. Data related to the fundamental properties of the feedstocks, as well as their suitability for processing with existing technology, are rarely found in the literature. Because of this, attempts to use SW in energy generation has been met with obstacles. In addition to waste energy, Indonesia, which has a water area around two-third of the overall space, has great potential for producing microalgae-based fuels. However, there has been little discussion of the microalgal potential for fuel generation in Indonesia. There is a need to investigate the potential of co-thermal conversion between waste and microalgae in light of the importance of providing alternative energy to replace fast-depleting fossil fuels.

Among the various thermochemical conversion methods, direct combustion is currently the most widely used option. Combustion comprises over 97% of the world's bio-energy generation [27]. The popularity of this method for biomass is due to reasons such as fuel flexibility, high heat transfer, and combustion efficiency [25]; whereas for solid waste, combustion also offers advantages, such as volume decrease of 90–95% [28, 29], mass reduction of 70%, perfect disinfection, and significant energy recovery [29].

Investigations into the combustion of single species of the microalgae *Chlorella vulgaris* [30], *Scenedesmus almeriensis* [31], *Nannochloropsis gaditana* [32], and *Nannochloropsis oculata* [3] have discovered various patterns during the thermal decomposition process. It has been thought that variances in the organic and mineral compounds in the typical species of microalgae lead to differences in thermal degradation. However, studies on the co-combustion of *Scenedesmus almeriensis* and lignocellulosic biomass [31], *Chlorella vulgaris* and textile dyeing sludge [33], and *Chlorella protothecoides* and rice straw [34] have found that a material's composition does have an effect on its combustion performance. To date, the co-combustion of microalgae and solid waste has not

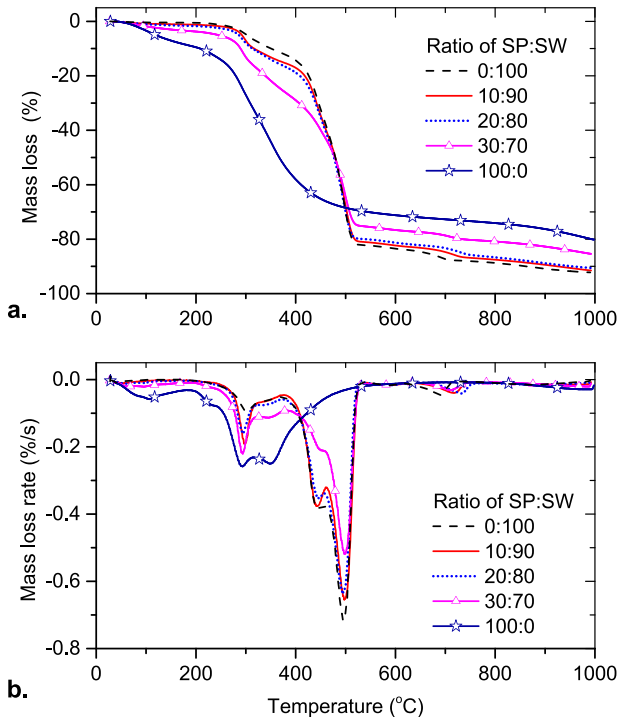

Figure 3. The curves of the various blends ratio of SP and SW at a heating rate of 40 °C/min: a. TG curves, b. DTG curves.

been performed, with the exception of *Chlorella protothecoides* and municipal solid waste under N_2/O_2 and CO_2/O_2 atmospheres [35]. This investigation revealed that the addition of microalgae improved municipal solid waste combustion. To the best of our knowledge, the co-combustion of SP and SW has not been studied. To extend the possible utilization of microalgae as fuel, with the overarching goal of recovering energy from SW, an in-depth study on the co-combustion of both materials was conducted.

This work investigated the behavior of SP and SW, both as individual materials and as a blend during the combustion process in non-isothermal conditions using thermogravimetric (TG) analysis. The temperature parameters that describe the decomposition of the material as the function of temperature were determined from the TG curves and the differential thermogravimetric (DTG) curves. Based on these curves, the kinetic parameters were evaluated using the fitting model proposed by Coats-Redfern and Horowitz-Metzger.

2. Materials and methods

2.1. Materials preparation

SP was cultivated by the Center for Development of Brackishwater Aquaculture (Balai Besar Pengembangan Budidaya Air Payau [BBPBAP]), Jepara, Indonesia. After harvesting, the biomass sediment was subjected to heat using an oven at 100 °C for 24 h to evaporate the water. The dry biomass chunks were then crushed and sieved through a mesh size of 40 (420 μm) to achieve a pulverized dry biomass, and the powder was stored in a tightly insulated bottle.

Around 19 kinds of synthetic materials composed of SW were collected. These materials were detergent packs, banners, mineral bottles, Styrofoam, shampoo bottles, mattresses, plastic bags, rice bags, jeans, water pipes, a plastic rice wrapper, sponges, flip-flops, oil bottles, jerrycans, a motorcycle body, synthetic leather, a bottle of liquid floor cleaner, and pieces of thick plastic. The samples were thoroughly cleaned and sun-dried for two days during the dry season. The samples were individually grated to powders and sieved to achieve a size of less than 40 mesh (420 μm). Following this, 19 samples with the same mass ratio were mixed. The mixing process was performed mechanically by pouring each of the 19 materials with the same mass ratio into a mortar, and grinding and mixing under low pressure. The blended materials were continuously mixed by shaking in a tightly sealed bottle to achieve a homogeneous SW blend. The final result was denoted as the SW.

Prior to testing, the SP and SW were blended in ratios of 0:100, 10:90, 20:80, 30:70, and 100:0 (wt,%) using a similar method as the SW mixing process. The ultimate and proximate results of SP and SW are listed in Table 1. The calorific values of both materials were determined through the instrumentality of adiabatic bomb calorimeters. 0.5 g of the samples were experimented with 99.5% pure oxygen for 10 min. The SP's protein and lipid contents were respectively determined by the Kjeldahl and Soxhlet methods, and the carbohydrate was calculated by difference as 100%-protein-lipid (by dry weight and ash-free basis) [36, 37].

2.2. Thermogravimetric experiment

A simultaneous thermogravimetric analyzer (METTLER TOLEDO TGA/DSC1) was used to evaluate the decomposition of the samples

Table 2. Characteristic temperatures and maximum mass loss rate of all samples at a various heating rate.

β(°C/min)	Samples	Zone I				Zone II			
		Ti (°C)	Tmax (°C)	Tf (°C)	Mmax (%/s)	Ti (°C)	Tmax (°C)	Tf (°C)	Mmax (%/s)
10	0SP/100SW	235.921	277.558	365.906	-0.0352	365.906	446.784	482.233	-0.0969
	10SP/90SW	233.830	271.602	361.691	-0.0331	361.691	458.291	484.135	-0.1269
	20SP/80SW	230.853	276.45	359.076	-0.0375	359.076	477.135	505.107	-0.1722
	30SP/70SW	228.176	275.125	358.485	-0.0354	358.485	477.694	506.909	-0.1784
	100SP/0SW	168.894	275.847	294.212	-0.0637	294.212	316.792	512.357	-0.0625
20	0SP/100SW	237.857	289.347	370.007	-0.0654	370.007	486.141	510.877	-0.3952
	10SP/90SW	235.322	287.431	368.068	-0.0983	368.068	486.672	512.433	-0.3409
	20SP/80SW	233.061	285.17	367.122	-0.0706	367.122	489.141	515.731	-0.3383
	30SP/70SW	230.259	281.384	366.443	-0.0743	366.443	481.256	516.47	-0.2879
	100SP/0SW	172.682	283.479	302.539	-0.1272	302.539	327.666	522.684	-0.1173
40	0SP/100SW	239.703	300.19	375.911	-0.0929	375.911	496.809	532.677	-0.7172
	10SP/90SW	237.703	296.771	373.337	-0.1914	373.337	497.431	533.483	-0.6551
	20SP/80SW	235.741	293.434	372.031	-0.1598	372.031	493.761	534.458	-0.6347
	30SP/70SW	232.394	293.707	370.31	-0.2205	370.31	497.323	535.395	-0.5187
	100SP/0SW	185.057	293.813	313.509	-0.2585	313.509	349.114	550.54	-0.2499

Ti: the temperature of initial decomposition at the related zone. Tmax, the temperature of maximum mass loss rate at the related zone. Tf: temperature of the completed decomposition at the related zone. Mmax: the maximum mass loss rate at the related zone.

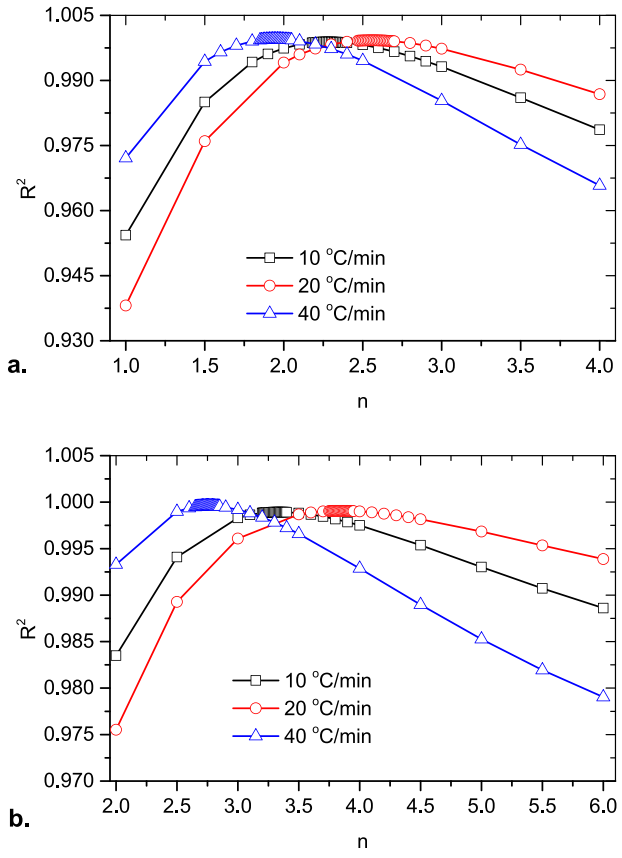

Figure 4. The $R^2 - n$ curves of the SP at various heating rates: a. Coats-Redfern, b. Horowitz-Metzger.

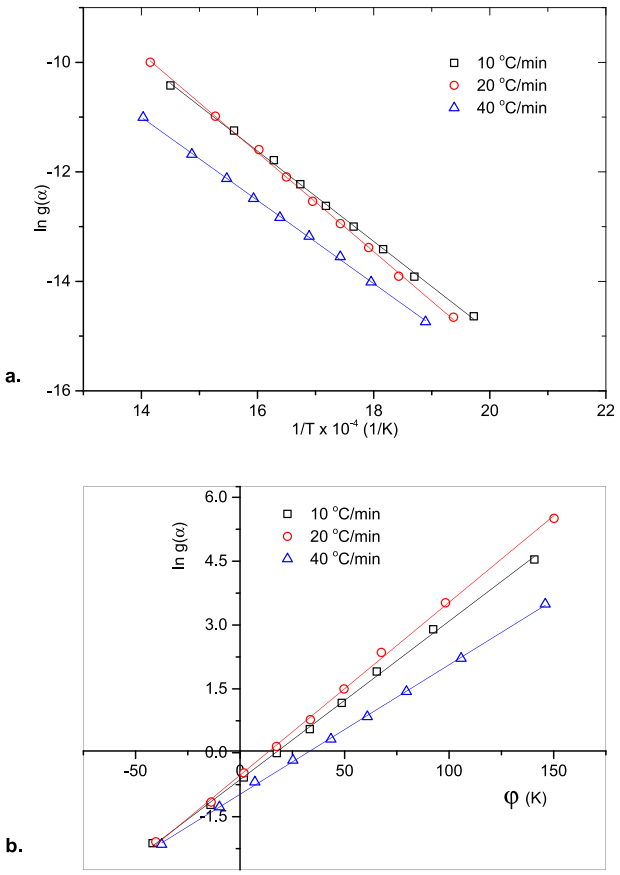

Figure 5. Linear regression of the final plot of the SP: a. Coats-Redfern, b. Horowitz-Metzger.

during the heating process under an oxidative atmosphere with a flow rate of 100 ml/min to determine whether the atmosphere was appropriate for combustion. For every experiment, approximately 10 mg of the sample was loaded into a ceramic crucible and inserted into a furnace. The samples experienced non-isothermal heating from room temperature to 1000 °C at the various heating program of 10, 20 and 40 °C/min. The thermogravimetric (TG) and differential scanning calorimetry data were recorded with a computer working in synchronization with the furnace. The differential thermogravimetry (DTG) data generated from the first derivative of the TG represented the mass loss rate of the materials in line with escalating time or temperature. The thermal behavior and characteristic parameters of the relevant samples were determined according to the TG and DTG data.

2.3. Kinetic method

It was necessary to examine the kinetic parameters in order to achieve a comprehensive understanding of how SP, SW, and their blends behaved during the combustion process. The rate of solid reaction that undergoes thermal attack is commonly expressed as an Arrhenius equation, as follows:

$$\frac{d\alpha}{dt} = k(T)f(\alpha) = A\exp\left(\frac{-E}{RT}\right)f(\alpha) \tag{1}$$

In Eq. (1), $k(T)$ is the rate constant, $f(\alpha)$ expresses the supposed model of the reaction mechanism, A (s^{-1}) is the frequency factor, E (kJ/mol) is the apparent activation energy, R(8.314 J/mol K) is the universal gas constant, T (K) is the absolute reaction temperature, α is the lost mass fraction, and $d\alpha/dt$ represents the conversion rate.

The extent of conversion (α), which represents the mass loss fractions of the sample material, is stated as the following equation:

$$\alpha = 1 - \frac{m_t - m_f}{m_i - m_f} = \frac{m_i - m_t}{m_i - m_f} \tag{2}$$

where m_i (mg) is the initial mass of the sample; m_t (mg) is the sample's remaining mass at time t; m_f (mg) is the final mass of the sample that refers to the end of the reaction.

For the non-isothermal experiment, the alteration of temperature in association with the time extension denotes the heating rate $dT/dt = \beta$. Substituting Eq. (1) with $dt = dT/\beta$ and defining the nth order reaction model results in $f(\alpha) = (1-\alpha)^n$, and leads to a non-isothermal expression, as follows:

$$\frac{d\alpha}{(1-\alpha)^n} = \frac{A}{\beta}e^{\frac{-E}{RT}}dT \tag{3}$$

On the basis of Eq. (3), the kinetic parameters were evaluated according to the fitting method proposed by Coats-Redfern and Horowitz-Metzger.

3. Results and discussions

Table 1 revealed the fundamental properties of SP and SW based on ultimate, proximate, and calorific value analyses. To simplify the analysis of the results, the thermal test results are presented into two sections, the first for individual fuel and the second for mixed fuel.

3.1. Individual fuels

The TG-DTG curves of the SP and SW at different heating rates are represented in Figures 1 and 2, respectively. The SP biomass sample decomposed in three different stages. The first stage corresponded to water removal from the biomass, as previously reported in the literature

Table 3. The kinetic parameters of the SP combustion.

Methods	β (°C/min)	Trendline equation	R^2	Kinetic parameters		
				E (kJ/mol)	log A (1/min)	n
Coats-Redfern	10	$y = -8243.6x + 1.569$	0.999	68.54	5.59	2.28
	20	$y = -9050.5x + 2.835$	0.999	75.25	6.49	2.56
	40	$y = -8243.6x + 1.569$	0.999	63.14	5.32	1.95
	Average		0.999	68.98	5.80	2.26
Horowitz-Metzger	10	$y = 0.0372x - 0.631$	0.999	93.19	10.25	3.43
	20	$y = 0.0406x - 0.525$	0.999	104.48	10.66	3.84
	40	$y = 0.0304x - 0.975$	0.999	81.22	10.68	2.76
	Average		0.999	92.96	10.53	3.34

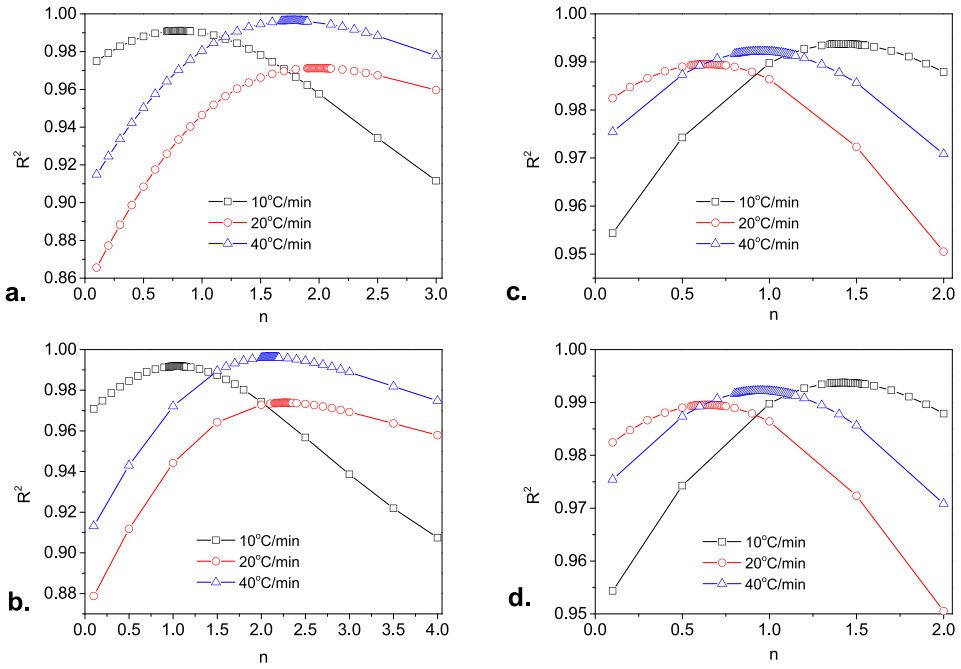

Figure 6. The $R^2 - n$ curves of the SW at various heating rates: a. Zone I of Coats-Redfern, b. Zone I of Horowitz-Metzger, c. Zone II of Coats-Redfern, d. Zone II of Horowitz-Metzger.

[3, 38, 39]. This stage began at room temperature and finished at around 170 °C (depending on the heating rate) in that the finishing temperature shifted to a higher temperature in line with the increasing heating rate. In this stage, it is thought that the cell structure underwent thermal cleavage, which promoted the thermal unfolding of the proteins and partly released as light volatile [32].

The second stage began at around 170 °C and ended at about 530 °C. Two sub-basin peaks of DTG curves were noted at this stage. The first correlated with the degradation and combustion of carbohydrate and a portion of protein, whereby both components were thermally degraded in the merged zone, and the second was associated with further decomposition and combustion of protein together with lipid. This observation is thought to be due to the fact that the temperature degradation of lipids is higher than proteins and carbohydrates [40]. The completion of the second stage resulted in char formation.

The third stage, characterized by a slight loss of mass, was thought to be due to further decomposition and oxidation of the carbonaceous materials in the char [41]. Additionally, both TG and DTG curves of Figure 1 also indicated the appearances of the last thermal degradation process of the samples at a temperature higher than 800 °C. By giving more attention to the TG curve Figure 1a, it would be found that around 74% of the material had been degraded thermally from the initial process until the temperature of 800 °C. Synchronizing this TG result with proximate data, it can be understood that most of the organic matter in the biomass, which is represented as VM and FC, has decomposed in this temperature range, but the carbon component is not entirely decomposed and burned. The main reason for this judgment was due to the fact that VM was more reactive than FC material. Therefore, it was strongly believed that the sharp decline of the TG curve above 800 °C was correlated with the further combustion of the rest of carbonaceous materials in the char and the decomposition of the mineral matter at a high temperature. The similar phenomena had been reported previously by Lopez-Gonzalez et al. [42] for the combustion process of *Nannochloropsis gaditana* and Sukarni et al. [3, 43] for the *Nannochloropsis oculata* microalgae. Deep scrutinizing had been presented in the latter reference, and the result indicated that the decomposition at a temperature higher than 800 °C was correlated with the dissociation alkali carbonate, mainly Na_2CO_3. Through the complex reaction mechanism within the ash at a high temperature, the dissociated Na_2CO_3 reacted with CaO and SiO_2 and creating a new compound of $Ca_6Na_2O_{15}Si_4$ [43]. The in-depth investigation of this SP sample's combustion at high temperatures should be performed in future work.

In SW combustion, Figure 2 suggests that there were three stages of thermal degradation in the combustion process. The first stage started from room temperature to around 200 °C and was associated with the releasing of light volatile and very low moisture content.

The second stage began at about 200 °C and completed at a range of 480–530 °C (depending on the heating rate). This stage correlated with

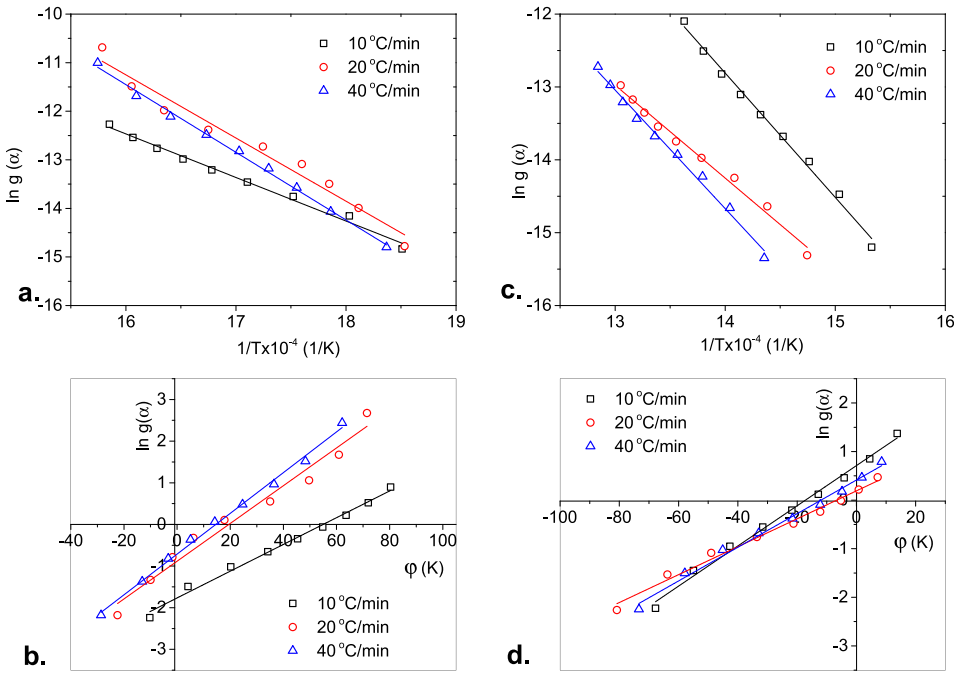

Figure 7. Linear regression of the final plot of the SW: a. Zone I of Coats-Redfern, b. Zone I of Horowitz-Metzger, c. Zone II of Coats-Redfern, d. Zone II of Horowitz-Metzger.

the main release and combustion of organic volatile components [44]. A thorough scrutiny of the second stage showed that there were two main sub-basins in the DTG curves. The first sub-basin, which peaked at around 300 °C, was associated with the thermal degradation of polyvinylchloride (PVC) and the second, which peaked at about 500 °C, corresponded to the massive degradation of various components of the SW, such as polystyrene (PS), polyethylene (PE), polycarbonate (PC), polyamide (PA), polypropylene (PP), polyethylene terephthalate (PET), and the second step of PVC decomposition [45].

The third stage of SW decomposition was characterized by a slight mass loss at around 500 °C until the process completed at 1000 °C. This stage was also indicated by the emergence of a small basin that peaked at around 675 °C. Tang et al. [46] found that the combustion of tire rubber, leather, and PVC in 80% N_2/20%O_2 had respective peaks of 780, 740, and 700 °C. Ren and Zhang [44] observed that waste plastic combustion had a first peak at 395 °C and a second peak at 665 °C. In line with previous research findings, we observed the formation of a small basin that peaked at around 675 °C and was associated with a slight

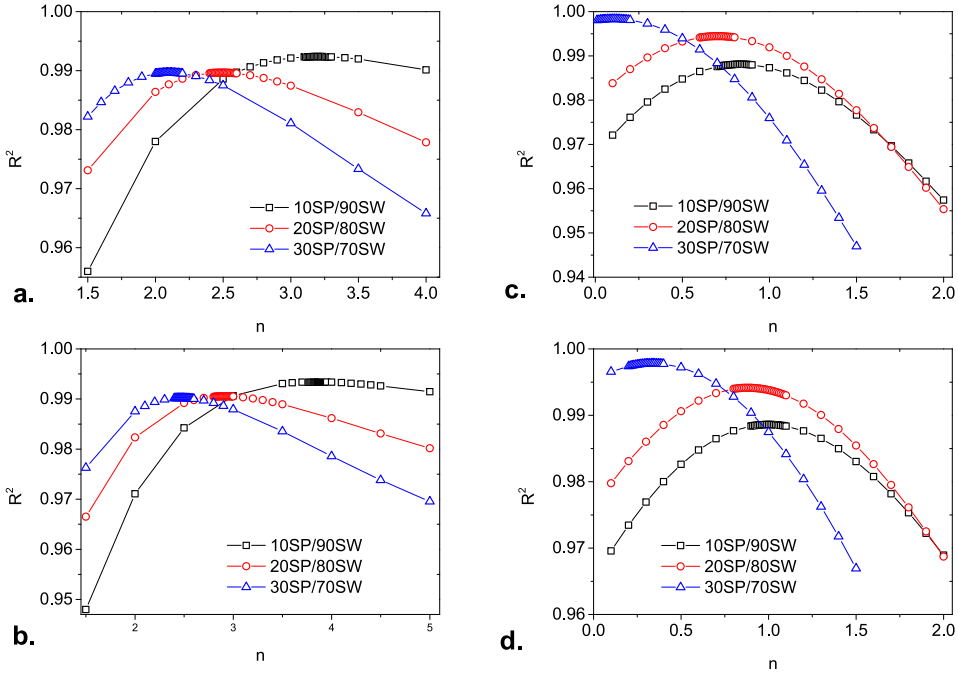

Figure 8. The $R^2 - n$ curves of the blended fuels at a heating rate of 40 °C/min: a. Zone I of Coats-Redfern, b. Zone I of Horowitz-Metzger, c. Zone II of Coats-Redfern, d. Zone II of Horowitz-Metzger.

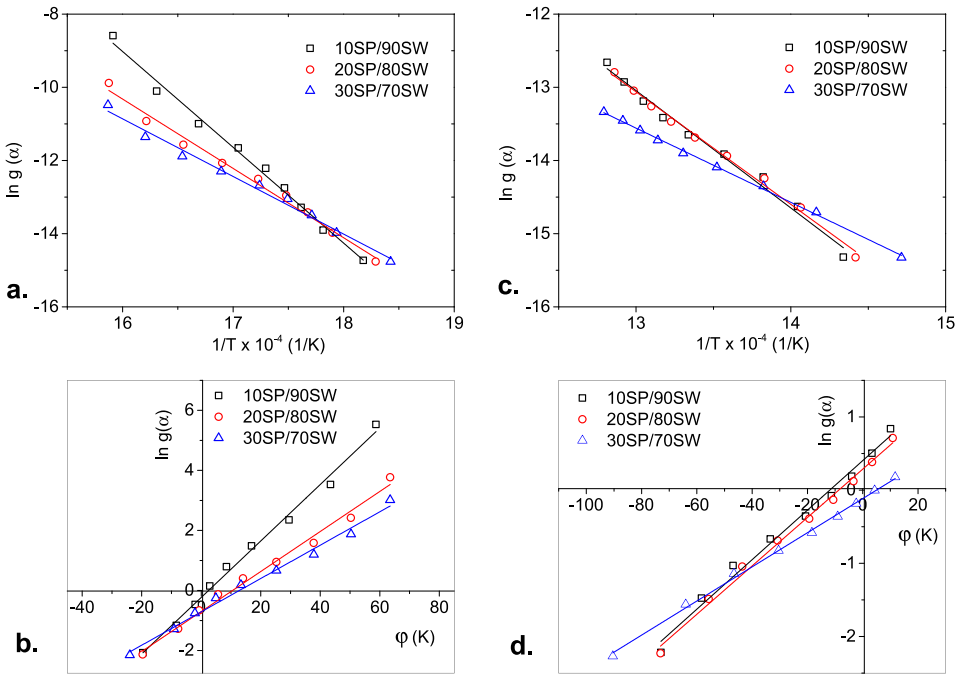

Figure 9. Linear regression of the final plot of the blended fuels at a heating rate of 40 °C/min: a. Zone I of Coats-Redfern, b. Zone I of Horowitz-Metzger, c. Zone II of Coats-Redfern, d. Zone II of Horowitz-Metzger.

degradation and further combustion of char and fixed carbon originating from the PVC ingredients in the SW. This result was in agreement with Lin et al. [47].

3.2. Blended fuels

The TG and DTG curves of the blend are depicted in Figure 3. Both the TG and DTG curves revealed that three stages also emerged for the blended samples.

In the first stage, the pronounced basin of the DTG curves (Figure 3b) gradually developed in line with the increasing proportion of SP in the blended fuel. As shown in Table 1, the moisture content in the SP was higher than in the SW; therefore, increasing the SP sample in the mixture significantly influenced the moisture level in the blended fuel.

It can be observed from the TG curves (Figure 3a) that increasing the SP content in the blended fuels led to the temperature of devolatilization to decrease. In harmony with the TG curves, it was also observed in the second stage of the DTG curves (Figure 3b) that the addition of SP facilitated a decrease in temperature in the initial decomposition process. This lesser initial decomposition temperature indicated that the addition of SP promoted the thermal degradation of the material. The microalgae, which were composed of the three main components of carbohydrates, proteins, and lipids [48], decomposed at a temperature range of 200–600 °C, which varied depending on the heating rate [39]. Grammelis et al. [45] reported an initial decomposition temperature of various plastic materials of 254–354 °C. Textile material was found to thermally decompose at 249 °C [49]. In the present work, it was found that an individual sample of SP began to decompose at a temperature of around 170 °C. This result confirmed that the SW material was more thermally stable than microalgal biomass and that SP biomass addition decreased its thermal stability.

The TG curves revealed that the mass loss of the blended fuels was higher than pure SW at a temperature of below 480 °C. At a temperature above 480 °C, an increasing SP content led to reduced mass loss and produced more leftover materials in line with higher SP in the mixture. These results were in agreement with the proximate results, in which the ash content of the SP was higher than the SW, but disagreed with results obtained by Tang et al. [35], which was likely due to differences in the fundamental characteristics of the algae and MSW used by Tang et al. compared to the SP and SW used in this study, as seen in the ultimate and proximate analysis.

From the DTG curves, two distinct sub-basins were observed in the second stage. In the first sub-basin, the mass loss rate increased gradually in line with the increasing SP in the mixture. It is thought that the materials in the microalgae had a more thermally unstable structure that led to easier degradation at a given temperature and promoted more mass release in the volatile form. The carbohydrates and proteins in the algal biomass also played a significant role in this zone. Conversely, in the second sub-basin, it was observed that the massive degradation of the materials decreased gradually in relation to the increasing content of SP in the mixture. The peaks of DTG curves at around 497 °C became less apparent, owing to the increase of low reactive combustible ingredients in the algae. This indicated that materials that remained after the first sub-basin, which were mainly lipids [39, 50], decomposed at a lower rate than the SW materials.

3.3. Kinetic evaluation

The fundamental objective of the kinetic evaluation is to determine the minimum amount of energy that must be obtained by an atomic system for it to take place in the reaction [51]. This parameter represented the difficulty of the chemical reaction completion and called as activation energy.

The various chemical compositions that exist in a multi-component solid material generate a chemically complex reaction during the thermal decomposition of materials that are simultaneously pyrolyzed and oxidized [3]. Hence, determining the best reaction kinetics that represent the actual reaction mechanism is difficult. For this reason, simplifying the reaction process by lumping the complicated multiple reactions that occur at a certain temperature range as an *n*th order reaction is reasonable [52].

In this work, the kinetic evaluation was performed in the second stage, in which decomposition and combustion took place. As previously discussed, there were two sub-basins in this stage. Therefore, the

Table 4. The kinetic parameters of the SW and blended fuels combustion according to the Coats-Redfern.

Samples	β (°C/min)	Zone	Trendline equation	R^2	Kinetic parameters		
					E (kJ/mol)	log A (1/min)	n
0SP/100SW	10	I	$y = -8966.9x + 1.881$	0.991	74.55	5.77	0.81
		II	$y = -17066x + 11.083$	0.994	141.88	10.05	1.22
	20	I	$y = -13006x + 9.559$	0.971	108.13	9.57	1.99
		II	$y = -12753x + 3.603$	0.989	106.03	6.97	0.48
	40	I	$y = -13931x + 10.837$	0.996	115.82	10.45	1.78
		II	$y = -16274x + 8.114$	0.992	135.30	9.34	0.78
	Average	I		0.986	99.50	8.60	1.53
		II		0.992	127.74	8.79	0.83
10SP/90SW	10	I	$y = -10070x + 4.204$	0.982	83.72	6.82	1.23
		II	$y = -15015x + 7.714$	0.998	124.83	8.53	0.82
	20	I	$y = -25919x + 33.2$	0.986	215.49	20.13	3.54
		II	$y = -14652x + 6.221$	0.990	121.81	8.17	0.67
	40	I	$y = -26187x + 32.878$	0.992	217.72	20.30	3.20
		II	$y = -16028x + 7.791$	0.988	133.26	9.19	0.84
	Average	I		0.987	172.31	15.75	2.66
		II		0.992	126.63	8.63	0.78
20SP/80SW	10	I	$y = -17252x + 18.007$	0.983	143.44	13.05	2.56
		II	$y = -13341x + 4.644$	0.988	110.92	7.14	0.56
	20	I	$y = -19000x + 20.645$	0.984	157.97	14.55	2.70
		II	$y = -15907x + 8.068$	0.979	132.25	9.00	0.99
	40	I	$y = -18954x + 20.005$	0.990	157.58	14.57	2.49
		II	$y = -15377x + 6.928$	0.995	127.85	8.80	0.70
	Average	I		0.986	153.00	14.06	2.58
		II		0.987	123.67	8.31	0.75
30SP/70SW	10	I	$y = -14396x + 12.615$	0.977	119.69	10.64	2.15
		II	$y = -13108x + 4.280$	0.989	108.98	6.98	0.49
	20	I	$y = -14105x + 11.692$	0.980	117.26	10.53	2.04
		II	$y = -15419x + 7.546$	0.992	128.19	8.77	0.86
	40	I	$y = -15751x + 14.34$	0.990	130.95	12.03	2.10
		II	$y = -10139x - 0.377$	0.998	84.30	5.44	0.11
	Average	I		0.982	122.63	11.07	2.10
		II		0.993	107.16	7.06	0.49

temperature characteristics for kinetic evaluation were divided into the first sub-basin (Zone I) and second sub-basin (Zone II), as depicted in Table 2.

The temperature ranges, as described in Table 2, were subject to kinetic evaluation using Eq. (4). The conversion (α) in the interval of 0.1–0.9 from certain zones that were taken into consideration was studied in order to guarantee that this kinetic evaluation could be characterized as the kinetics of complicated multiple reactions in the related zones. Two fitting techniques proposed by Coats-Redfern and Horowitz-Metzger were applied in this study.

The fitting-models allowed for the determination of the kinetic parameters by choosing the appropriate reaction model $f(\alpha)$ for the decomposition of biomass considered during the thermochemical process. In the fitting methods, the kinetics evaluation was performed under a single heating rate, which is disadvantageous because the activation energy varied with the heating rate due to the effect of mass or energy transfer [53]. However, applying model fitting to datasets from multiple heating rates could increase the robustness of the results [54, 55]. Several research papers have been published using this technique. For example, Gill et al. [56] performed a kinetic analysis of the co-combustion of a coal-biomass blend using a single heating rate of 15 °C/min. Pickard et al. [54] conducted a kinetic evaluation using two heating rates of 10 and 40 K/min. Yorulmaz and Atimtay [57] carried out a kinetic calculation using three heating rates of 10, 20 and 30 °C/min. In this work, the kinetic parameters were evaluated in three heating programs of 10, 20 and 40 °C/min.

Using the Coats-Redfern method, the integration of Eq. (3) resulted in an exponential integral. By applying the Taylor series method and following the linearization, the final equation form was produced:

$$\ln g(\alpha) = -\frac{E}{RT} + \ln\frac{AR}{\beta E} \tag{4}$$

where:

if $n = 1$ then $g(\alpha) = -(\ln(1-\alpha))/T^2$

if $n \neq 1$ then $g(\alpha) = (1-(1-\alpha)^{(1-n)})/((1-n)T^2)$

The Horowitz-Metzger method was also applied to Eq. (3) and generated a linear equation as follows:

$$\ln g(\alpha) = \left(\ln\left(\frac{ART_{max}^2}{\beta E}\right) - \frac{E}{RT_{max}}\right) + \frac{E\phi}{RT_{max}^2} \tag{5}$$

where:

if $n = 1$ then $g(\alpha) = -\ln(1-\alpha)$

if $n \neq 1$ then $g(\alpha) = (1-(1-\alpha)^{(1-n)})/(1-n)\phi = T - T_{max}$, which T_{max} is the maximum mass loss rate temperature.

Açikalin [52, 58] proposed a method for determining the proper reaction order (n) value. On the basis of Eqs. (4) and (5), plotting $\ln g(\alpha)$ versus $1/T$ and $\ln g(\alpha)$ versus ϕ at the selected n range, respectively, yielded a straight line with a correlation coefficient of R^2. The most appropriate n value in correlation with the best linear plot was indicated by the highest value of the correlation coefficient (R^2) [59, 60]. With this

Table 5. The kinetic parameters of the SW and blended fuels combustion according to the Horowitz-Metzger method.

Samples	β (°C/min)	Zone	Trendline equation	R^2	Kinetic parameters		
					E (kJ/mol)	log A (1/min)	n
0SP/100SW	10	I	$y = 0.0321 - 1.765$	0.992	80.93	9.70	1.05
		II	$y = 0.0413 + 0.711$	0.994	178.15	11.35	1.43
	20	I	$y = 0.0453 - 0.883$	0.974	119.04	10.57	2.27
		II	$y = 0.0287 + 0.191$	0.990	137.62	11.36	0.65
	40	I	$y = 0.0489 - 0.712$	0.996	133.50	11.01	2.12
		II	$y = 0.0346 + 0.315$	0.992	170.62	11.86	0.96
	Average	I		0.987	111.16	10.42	1.81
		II		0.992	162.13	11.52	1.01
10SP/90SW	10	I	$y = 0.0363 - 1.661$	0.985	89.56	9.78	1.47
		II	$y = 0.0361 + 0.532$	0.997	160.23	11.24	1.02
	20	I	$y = 0.098 - 0.190$	0.988	255.83	11.20	4.35
		II	$y = 0.0323 + 0.330$	0.991	155.05	11.47	0.84
	40	I	$y = 0.0941 - 0.232$	0.993	253.82	11.49	3.84
		II	$y = 0.0338 + 0.403$	0.989	166.91	11.85	1
	Average	I		0.989	199.73	10.82	3.22
		II		0.992	160.73	11.52	0.95
20SP/80SW	10	I	$y = 0.0643 - 0.698$	0.985	161.45	10.46	3
		II	$y = 0.0304 + 0.213$	0.989	142.02	11.07	0.72
	20	I	$y = 0.0688 - 0.662$	0.986	178.05	10.83	3.17
		II	$y = 0.0345 + 0.596$	0.981	166.37	11.62	1.14
	40	I	$y = 0.0677 - 0.700$	0.991	177.77	11.13	2.92
		II	$y = 0.033 + 0.287$	0.994	161.49	11.78	0.88
	Average	I		0.987	172.42	10.80	3.03
		II		0.988	156.62	11.49	0.91
30SP/70SW	10	I	$y = 0.0525 - 0.999$	0.980	131.01	10.24	2.47
		II	$y = 0.0299 + 0.176$	0.990	139.91	11.05	0.65
	20	I	$y = 0.0502 - 1.078$	0.982	128.13	10.50	2.35
		II	$y = 0.0345 + 0.496$	0.992	162.94	11.56	1.04
	40	I	$y = 0.0555 - 0.711$	0.990	148.29	11.05	2.46
		II	$y = 0.0233 - 0.116$	0.998	114.93	11.46	0.34
	Average	I		0.984	135.81	10.59	2.42
		II		0.993	139.26	11.35	0.67

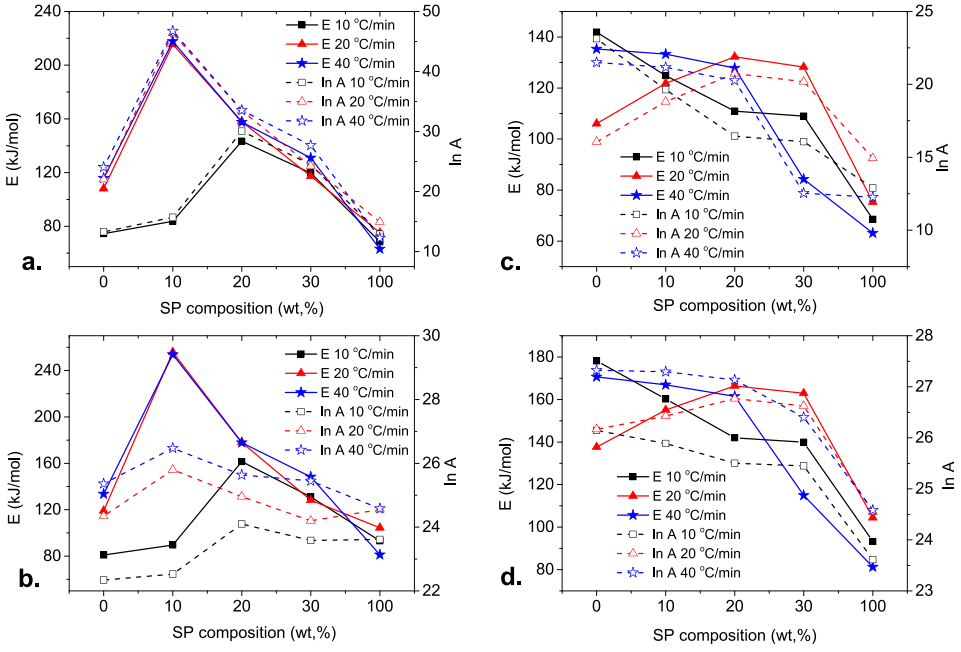

Figure 10. The relationship between kinetic parameters of (E and A) and the SP composition in the blended fuel at various heating rates: a. Zone I of Coats-Redfern, b. Zone I of Horowitz-Metzger, c. Zone II of Coats-Redfern, d. Zone II of Horowitz-Metzger.

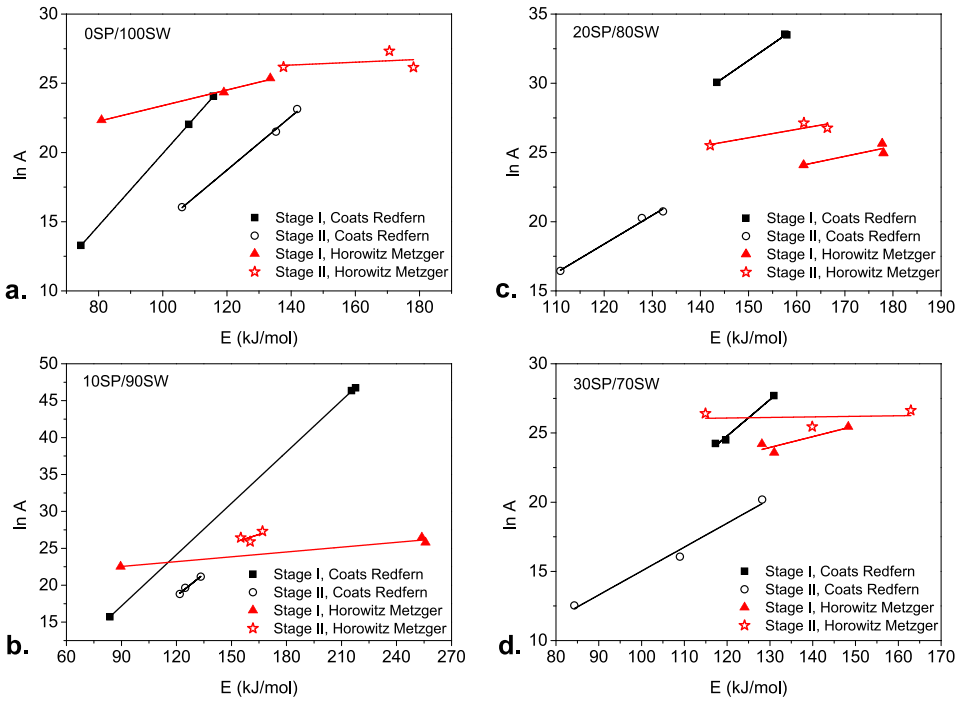

Figure 11. The kinetic compensation effect of SP and SW co-combustion at a various blending ratio: a. 0SP/100SW, b. 10SP/90SW, c. 20SP/80SW, d. 30SP/70SW.

Table 6. The linear regression parameters of the kinetics compensation effect.

Samples	Zone	Coats-Redfern		Horowitz-Metzger	
		Trendline equation	R^2	Trendline equation	R^2
0SP/100SW	I	$\ln A = 0.261E - 6.179$	1.000	$\ln A = 0.057E + 17.741$	0.995
	II	$\ln A = 0.194E - 4.549$	0.998	$\ln A = 0.010E + 24.886$	0.107
10SP/90SW	I	$\ln A = 0.232E - 3.696$	1.000	$\ln A = 0.022E + 20.579$	0.971
	II	$\ln A = 0.200E - 5.502$	0.991	$\ln A = 0.080E + 13.726$	0.447
20SP/80SW	I	$\ln A = 0.241E - 4.450$	0.999	$\ln A = 0.072E + 12.415$	0.793
	II	$\ln A = 0.208E - 6.574$	0.991	$\ln A = 0.061E + 16.902$	0.844
30SP/70SW	I	$\ln A = 0.262E - 6.665$	0.990	$\ln A = 0.078E + 13.803$	0.801
	II	$\ln A = 0.173E - 2.256$	0.987	$\ln A = 0.004E + 25.589$	0.025

purpose in mind, the $R^2 - n$ curve was drawn, and the most appropriate n value was determined from the highest R^2. The most appropriate n value was then applied to calculate $\ln g(\alpha)$ at the selected α. The final plot of $\ln g(\alpha)$ versus $1/T$ (for Coats-Redfern method) and $\ln g(\alpha)$ versus ϕ (for the Horowitz–Metzger method) could be drawn in regard to the T at a corresponding α. The respective apparent activation energy and frequency factor were determined from the slope and interception of the final plot from the related zone.

In the case of SP, Zones I and II of the second stage were separated by unpronounced humps, as described by DTG curves in Figure 1b. Kinetic analysis of the SP was performed in the second stage as a single step reaction of the nth order, without considering Zones I and II as the separating step. This judgment was supported by the fact that only a single slope change was encountered on each TG curve (Figure 1a).

Table 2 shows that for the 100SP/0SW, the temperature ranges extended from the initial decomposition temperature (Ti) in Zone I to the completed decomposition temperature (Tf) in Zone II, and this was used for kinetics analysis. By selecting any n values, the plot of $\ln g(\alpha)$ versus $1/T$ (Coats-Redfern) and $\ln g(\alpha)$ versus ϕ (Horowitz-Metzger) was performed and resulted in various R^2 values. The plots of $R^2 - n$ at heating rates of 10, 20 and 40 °C/min are depicted in Figure 4a (Coats-Redfern) and 4b (Horowitz-Metzger) and were used to determine the most appropriate n. Using these n values, the final plots of $\ln g(\alpha)$ versus $1/T$ (Coats-Redfern) and $\ln g(\alpha)$ versus ϕ (Horowitz-Metzger) were drawn, and are shown in Figures 5a and 5b. Using the linear regression of these final plots, the apparent activation energy and frequency factor were evaluated from the slopes and intercepts, respectively. The kinetic parameters for the SP are depicted in Table 3.

In relation to the kinetic parameters of SP shown in Table 3, it was observed that the two kinetic methods showed a similar trend in apparent activation energy in regard to heating rate changes. The highest apparent activation energy occurred at 20 °C/min, the middle at 10 °C/min, and the smallest at 40 °C/min, with both Coats-Redfern and Horowitz-Metzger, have been given similar tendencies. It was found that the heating rate had a significant impact on apparent activation energy. The kinetic analysis also revealed that the Horowitz-Metzger method presented higher apparent activation energy than the Coats-Redfern method. These results were in agreement with previous findings [52, 58, 61, 62].

For the SW and the blended fuels, Zones I and II of the second stage were separated by pronounced humps of the DTG curves, as shown in Figure 3b. The TG curves in Figure 3a also specified that the two slope changes in the second stage indicated two-step reactions. Hence, every zone in the second stage was considered a single step reaction of nth order. The kinetic evaluation was performed separately for Zones I and II.

On the basis of the characteristic temperatures shown in Table 2, kinetic evaluations of the SW and blended fuels were performed by a similar procedure to SP. The $R^2 - n$ curves and the final plots of the SW are depicted in Figures 6 and 7, respectively. The $R^2 - n$ curves and final plots for the blended fuels at a heating rate of 40 °C/min are represented in Figures 8 and 9. The kinetic parameters at various heating rates are depicted in Table 4 (Coats-Redfern) and 5 (Horowitz-Metzger).

As shown in Tables 4 and 5, in general, adding microalgae to the SW significantly affected the apparent activation energy. For the individual SW, the average apparent activation energy in Zone I was 99.50 and 111.16 kJ/mol based on the Coats-Redfern and Horowitz-Metzger methods, respectively. An additional 10% SP added to the SW lead to an increased average apparent activation energy of the blended fuel that was 172.31 kJ/mol (Coats-Redfern) and 199.73 kJ/mol (Horowitz-Metzger). Increasing the proportion of SP from 10 to 20 and 30 (wt,%) of the fuel led to a decrease in the average apparent activation energy. In the 20SP/80SW mixture, the average apparent activation energies were 153.00 kJ/mol (Coats-Redfern) and 172.42 kJ/mol (Horowitz-Metzger). The average apparent activation energy of the 30SP/70SW mixture was 122.63 kJ/mol (Coats-Redfern) and 135.81 kJ/mol (Horowitz-Metzger). Overall, the average apparent activation energy in Zone I of the SW as an individual fuel was less compared to the blended fuels in the same zone. These results were in agreement with the results of Gao et al. [63] using a lignite coal and *Chlorella vulgaris* blend and with the result of Peng et al. [33] using a mixture of textile dyeing sludge and *Chlorella vulgaris*. Gao et al. found that microalgae addition from 30 to 70 (wt,%) significantly increased the activation energy; whereas Peng et al. identified that the activation energy of individual textile dyeing sludge was lower than that of a mixture, with the exception of a ratio of 40–60 (wt,%) microalgae. The results in this study revealed that a 10 (wt,%) microalgae addition resulted in the highest average apparent activation energy and that a 20 or 30 (wt%) addition resulted in lower average apparent activation energy than 10%. The order of the apparent activation energies in Zone I from the highest to the lowest were 10SP/90SW > 20SP/80SW > 30SP/70SW > 0SP/100SW, with both methods of Coats-Redfern and Horowitz-Metzger showing a similar trend. However, the results of this study, as well as those of Peng et al. [33], revealed that the activation energies did not increase linearly with increased microalgae content in the mixture, contrary to the results of Gao et al. [63]. These differences are thought to be due to different synergistic effects among the particles of various mixtures during the combustion process. This phenomenon should be explored in further depth in future research.

Tables 4 and 5 show that the presence of microalgae in Zone II in the mixture noticeably decreased in the average apparent activation energy. The higher the proportion of SP, the lower the average apparent activation energy. In Zone II, the increasing proportion of the microalgae was always followed by a decrease in the average apparent activation energy, contrary to Zone I. It is thought that interactions between the lipid content in the microalgae provoked the degradation and combustion of various SW material components.

As shown in Tables 4 and 5, another kinetic parameter that indicated the chemical reaction rate was frequency factor (A). This parameter represents a measure of the frequency of collisions of all molecules during the thermochemical conversion process, without considering their energy level [64, 65]. The exponential term of the Arrhenius formula in Eq. (1) denotes the fraction of collisions that possessed adequate kinetic energy to produce a reaction; the rate constant, $k(T)$, reflects the frequency of successful collisions [65]. Based on the Coats-Redfern method, it was found that the frequency factor of the blended fuel in Zone II was lower than Zone I. This phenomenon was caused by the degradation of carbohydrates and proteins in the microalgae, followed by thermal cleavage of the lipids. The lipids subsequently provoked the SW material to thermally crack and resulted in a higher reaction rate in the blended materials in Zone II. This result differs from the Horowitz-Metzger results, in which the frequency factor between Zones I and II was almost equal. Considering these results with the preceding DTG curve in Figure 3b, the Coats-Redfern method is thought to be the most appropriate model, as in Zone II there was higher reaction rate (mass loss rate) than in Zone I. Tsamba et al. [66] explained that given small size sample particles led to effects of intra-particle heat transfer and diffusion can be ignored, and therefore determination of the kinetic parameters using the Coats-Redfern method is acceptable. An evaluation of E, A, and n using various methods was performed by Petrovic and Zavargo [67]. They found that the Coats-Redfern method resulted in around a 2% lower activation energy and frequency factor, which indicated that this method produced the fewest errors [57]. They also discovered considerable errors in the Horowitz-Metzger method for determining the activation energy and frequency factor, thought to be due to the improper numerical form of the Horowitz-Metzger formula [67]. However, they suggested that the robustness of the method and a lower risk of errors could be achieved by applying multiple heating rates [67].

The various vital kinetic parameters in this study provide a thorough evaluation and can be considered practical guidance for industrial applications. The increasing average apparent activation energy in Zone I and the decreasing apparent activation energy in Zone II in line with the rising proportion of the SP provides guidance on the minimum amount of energy required for initiating the combustion process in industrial furnaces. The frequency factor and reaction order values are a guide for estimating the reaction rate [50]. In addition, a non-integer order of reaction was found at every investigated zone, which demonstrated that the thermochemical conversion process of the samples took place in a complex reaction mechanism [68].

Employing the kinetic parameters presented in Tables 4 and 5 to the Arrhenius equation (Eq. (1)), subsequently, the rate of samples' reaction of any blend ratios could be estimated. For practical purposes, this chemical reaction rate is useful as a reference in determining a suitable combustion equipment design. Therefore, understanding the chemical reaction rate would help guide the proper sizing of a combustion chamber and the precise setting up of the control system to achieve the highest energy recovery, compliance with safety standards, and economic feasibility. A more detailed explanation of the relationship between kinetic parameters and designing a combustion reactor could refer to Date [69]. By this route, the SW could meet the most proper handling in terms of co-utilization with the SP for energy generation.

3.4. Compensation effects

Figure 10 presents the relationship between kinetic parameters (apparent activation energy and frequency factor) and the SP composition in the blended fuel at various heating rates. The apparent activation energy and the frequency factor exhibited the same behavior, whereby a decrease in apparent activation energy due to changes in the SP composition at a specified heating rate was always accompanied by a decrease in the frequency factor and vice versa. This indicated the existence of a kinetic compensation effect between E and A during the SP and SW blend combustion.

The phenomenon of the kinetic compensation effect has been previously discussed [65, 70]. The compensation effect complicates blended fuel combustion as the apparent activation energy and frequency factor play opposing roles in the rate of combustion. The decrease in apparent activation energy is favorable in thermochemical reactions, while a lower frequency factor leads to a decline in the combustion rate. However, the compensation effect shows that a decrease in apparent activation energy, which raises the rate of combustion at a given temperature, is compensated for by a decrease in the frequency factor. Therefore, determining the reactivity of the combustion with only the activation energy and frequency factor is inadequate [71]. Further investigation is critical in establishing the mechanism for this. Thermal studies have revealed that the reactivity of the thermochemical reaction (temperature sensitivity of

the reaction rate) is mostly determined by the activation energy [72], whereas the frequency factor is mostly related to the material structure [73], and this is dependent on and strongly linked with activation energy via a compensation effect and is, therefore, a less significant parameter compared with activation energy [72]. Tsamba et al. [66] reported that the sensitivity of the Arrhenius constant, $k(T)$, to the temperature is predominantly determined by the activation energy.

Many studies have found that the relationship between E and A can be expressed by the following equation [65, 74, 75, 76, 77]:

$$\ln A = aE + b \tag{6}$$

where a and b are the compensation coefficients.

In reference to Tables 4 and 5, the relationship between apparent activation energy E and frequency factor A is shown in Figure 11. Table 6 summarizes the results of the linear regression of the plot between apparent activation energy E and frequency factor A. Using the Coats-Redfern method, it was observed that very high correlation coefficients were encountered in Zones I and II. These results confirmed the existence of the kinetic compensation effect during the combustion of an SP and SW blend. Different results were found using the Horowitz-Metzger, where fewer correlation coefficients were noted for 0SP/100SW, 10SP/90SW, and 30SP/70SW in Zone II. The fewer correlation coefficients may have resulted from their frequency factors that did not noticeably change with different heating rates. Kinetic compensation effects have also been identified in the co-combustion of beetroot and switchgrass with coal [78], the thermal decomposition of wood and leaf samples in the air atmosphere [79], the combustion of various biomass [76], and the pyrolysis and combustion of coal [71].

4. Conclusions

The combustion behavior and kinetic parameters of the microalgae SP, synthetic wastes, and their blends were studied. Three stages of thermal degradation were encountered during temperature escalation from room temperature to 1000 °C. There were two zones of thermal degradation in the second stage of the blended materials, and this was also found for the SW. The mass loss rate of Zone I increased in line with the increasing proportion of microalgae in the mixture. Conversely, a higher content of microalgae in Zone II led to a decrease in the mass loss rate. The apparent activation energies in Zone I increased due to the presence of microalgae in the blended fuels, with the highest rate observed at 10SP/90SW. In Zone II, the increased content of microalgae was significantly affected by decreasing apparent activation energy. The existence of a kinetic compensation effect during the combustion process of the blended fuel was proven under the Coats-Redfern method for the overall ratio of the blend used in this work, in both Zones I and II.

Declarations

Author contribution statement

Sukarni Sukarni: Conceived and designed the experiments; Performed the experiments; Analyzed and interpreted the data; Wrote the paper.

Funding statement

Sukarni Sukarni was supported by Kementerian Riset Teknologi dan Pendidikan Tinggi Republik Indonesia (26.3.35/UN32.14/LT/2018, 188/SP2H/LT/DRPM/ 2019 and 188/SP2H/AMD/ LT/DRPM/2020).

Competing interest statement

The authors declare no conflict of interest.

Additional information

No additional information is available for this paper.

References

[1] BP Energy Outlook, 2019. https://www.bp.com/content/dam/bp/business-sites/en/global/corporate/pdfs/energy-economics/energy-outlook/bp-energy-outlook-2019.pdf. (Accessed 18 November 2019).
[2] S. Sukarni, S. Sumarli, I.M. Nauri, P. Purnami, A. Al Mufid, U. Yanuhar, Exploring the prospect of marine microalgae Isochrysis galbana as sustainable solid biofuel feedstock, J. Appl. Res. Technol. 16 (2018) 53–66.
[3] Sudjito Sukarni, N. Hamidi, U. Yanuhar, I.N.G. Wardana, Thermogravimetric kinetic analysis of Nannochloropsis oculata combustion in air atmosphere, Front. Energy 9 (2015) 125–133.
[4] Sumarli Sukarni, P. Puspitasari, H. Suryanto, R.F. Wati, Physicochemical characteristics of various inorganic combustible solid waste (ICSW) mixed as sustainable solid fuel, AIP Conf. Proc. (2017), 020066.
[5] M.A. Sokoto, R. Singh, B.B. Krishna, J. Kumar, T. Bhaskar, Non-isothermal kinetic study of de-oiled seeds cake of African star apple (Chrosophyllum albidum) using thermogravimetry, Heliyon 2 (2016).
[6] J. Lü, C. Sheahan, P. Fu, Metabolic engineering of algae for fourth generation biofuels production, Energy Environ. Sci. 4 (2011) 2451–2466.
[7] K. Ullah, M. Ahmad, Sofia, V.K. Sharma, P. Lu, A. Harvey, M. Zafar, S. Sultana, C.N. Anyanwu, Algal biomass as a global source of transport fuels: overview and development perspectives, Prog. Nat. Sci. Mater. Int. 24 (2014) 329–339.
[8] F. Fasaei, J.H. Bitter, P.M. Slegers, A.J.B. van Boxtel, Techno-economic evaluation of microalgae harvesting and dewatering systems, Algal. Res. 31 (2018) 347–362.
[9] L. Brennan, P. Owende, Biofuels from microalgae-A review of technologies for production, processing, and extractions of biofuels and co-products, Renew. Sustain. Energy Rev. 14 (2010) 557–577.
[10] E. Molina Grima, E.-H. Belarbi, F.G. Acién Fernández, A. Robles Medina, Y. Chisti, Recovery of microalgal biomass and metabolites: process options and economics, Biotechnol. Adv. 20 (2003) 491–515. http://www.ncbi.nlm.nih.gov/pubmed/14550018.
[11] P. McKendry, Energy production from biomass (part 2): conversion technologies, Bioresour. Technol. 83 (2002) 47–54.
[12] N. Uduman, Y. Qi, M.K. Danquah, G.M. Forde, A. Hoadley, Dewatering of microalgal cultures: a major bottleneck to algae-based fuels, J. Renew. Sustain. Energy 2 (2010).
[13] K.Y. Show, D.J. Lee, A.S. Mujumdar, Advances and challenges on algae harvesting and drying, Dry. Technol. 33 (2015) 386–394.
[14] L. Jin, T. Gebreegziabher, Z. Yu, A.O. Oyedun, Z. Yi, W. Maojian, C.W. Hui, Modeling and optimization of microalgae drying for power generation, Energy Procedia. 61 (2014) 168–171.
[15] K.K. Sharma, S. Garg, Y. Li, A. Malekizadeh, P.M. Schenk, Critical analysis of current microalgae dewatering techniques Critical analysis of current microalgae, Dewat. Tech. 4 (2017) 397–407.
[16] T. Ndikubwimana, J. Chang, Z. Xiao, W. Shao, X. Zeng, I.S. Ng, Y. Lu, Flotation: a promising microalgae harvesting and dewatering technology for biofuels production, Biotechnol. J. 11 (2016) 315–326.
[17] M. Musa, A. Doshi, R. Brown, T.J. Rainey, Microalgae dewatering for biofuels: a comparative techno-economic assessment using single and two-stage technologies, J. Clean. Prod. (2019).
[18] F.F. Madkour, A.E.-W. Kamil, H.S. Nasr, Production and nutritive value of Spirulina platensis in reduced cost media, Egypt, J. Aquat. Res. 38 (2012) 51–57.
[19] V. Anand, V. Sunjeev, R. Vinu, Catalytic fast pyrolysis of Arthrospira platensis (spirulina) algae using zeolites, J. Anal. Appl. Pyrolysis 118 (2016) 298–307.
[20] H. Desmorieux, J. Madiouli, C. Herraud, H. Mouaziz, Effects of size and form of Arthrospira Spirulina biomass on the shrinkage and porosity during drying, J. Food Eng. 100 (2010) 585–595.
[21] M.G. Mustafa, T. Umino, H. Nakagawa, The effect of Spirulina feeding on muscle protein deposition in red sea bream, Pagrus major, J. Appl. Ichthyol. 10 (1994) 141–145.
[22] D. Soletto, L. Binaghi, A. Lodi, J.C.M. Carvalho, A. Converti, Batch and fed-batch cultivations of Spirulina platensis using ammonium sulphate and urea as nitrogen sources, Aquaculture 243 (2005) 217–224.
[23] W. Shi, S. Li, G. Li, W. Wang, Q. Chen, Y. Li, X. Ling, Investigation of main factors affecting the growth rate of Spirulina, Optik 127 (2016) 6688–6694.
[24] W. Peng, Q. Wu, P. Tu, N. Zhao, Pyrolytic characteristics of microalgae as renewable energy source determined by thermogravimetric analysis, Bioresour. Technol. 80 (2001) 1–7.
[25] C. Gai, Z. Liu, G. Han, N. Peng, A. Fan, Combustion behavior and kinetics of low-lipid microalgae via thermogravimetric analysis, Bioresour. Technol. 181 (2015) 148–154.
[26] J.R. Jambeck, R. Geyer, C. Wilcox, T.R. Siegler, M. Perryman, A. Andrady, R. Narayan, K.L. Law, Plastic waste inputs from land into the ocean, Science 347 (2015) 768–771 (80-).
[27] A. Demirbas, Combustion characteristics of different biomass fuels, Prog. Energy Combust. Sci. 30 (2004) 219–230.
[28] C. Montejo, C. Costa, P. Ramos, M.D.C. Márquez, Analysis and comparison of municipal solid waste and reject fraction as fuels for incineration plants, Appl. Therm. Eng. 31 (2011) 2135–2140.

[29] M. Li, J. Xiang, S. Hu, L.-S. Sun, S. Su, P.-S. Li, X.-X. Sun, Characterization of solid residues from municipal solid waste incinerator, Fuel 83 (2004) 1397–1405.
[30] C. Chen, X. Ma, K. Liu, Thermogravimetric analysis of microalgae combustion under different oxygen supply concentrations, Appl. Energy 88 (2011) 3189–3196.
[31] R. López, C. Fernández, X. Gómez, O. Martínez, M.E. Sánchez, Thermogravimetric analysis of lignocellulosic and microalgae biomasses and their blends during combustion, J. Therm. Anal. Calorim. 114 (2013) 295–305.
[32] L. Sanchez-Silva, D. López-González, A.M. Garcia-Minguillan, J.L. Valverde, Pyrolysis, combustion and gasification characteristics of Nannochloropsis gaditana microalgae, Bioresour. Technol. 130 (2013) 321–331.
[33] X. Peng, X. Ma, Z. Xu, Thermogravimetric analysis of co-combustion between microalgae and textile dyeing sludge, Bioresour. Technol. 180 (2015) 288–295.
[34] Y. Tang, X. Ma, Z. Lai, Q. Yu, Oxy-fuel combustion characteristics and kinetics of microalgae and its mixture with rice straw using thermogravimetric analysis, Int. J. Energy Res. 42 (2018) 532–541.
[35] Y. Tang, X. Ma, Z. Lai, Thermogravimetric analysis of the combustion of microalgae and microalgae blended with waste in N(2)/O(2) and CO(2)/O(2) atmospheres, Bioresour. Technol. 102 (2011) 1879–1885.
[36] J. Wang, X. Ma, Z. Yu, X. Peng, Y. Lin, Studies on thermal decomposition behaviors of demineralized low-lipid microalgae by TG-FTIR, Thermochim. Acta 660 (2018) 101–109.
[37] S. Perazzoli, B.M. Bruchez, W. Michelon, R.L.R. Steinmetz, M.P. Mezzari, E.O. Nunes, M.L.B. da Silva, Optimizing biomethane production from anaerobic degradation of Scenedesmus spp. biomass harvested from algae-based swine digestate treatment, Int. Biodeterior. Biodegrad. 109 (2016) 23–28.
[38] S. Sukarni, S. Sumarli, I.M. Nauri, A. Prasetiyo, P. Puspitasari, Thermogravimetric analysis on combustion behavior of marine microalgae Spirulina platensis induced by MgCO3 and Al2O3 additives, Int. J. Technol. 10 (2019) 1174–1183.
[39] A. Agrawal, S. Chakraborty, A kinetic study of pyrolysis and combustion of microalgae Chlorella vulgaris using thermo-gravimetric analysis, Bioresour. Technol. 128 (2013) 72–80.
[40] D. López-González, M. Puig-Gamero, F.G. Acién, F. García-Cuadra, J.L. Valverde, L. Sanchez-Silva, Energetic, economic and environmental assessment of the pyrolysis and combustion of microalgae and their oils, Renew. Sustain. Energy Rev. 51 (2015) 1752–1770.
[41] A.M. Rizzo, M. Prussi, L. Bettucci, I.M. Libelli, D. Chiaramonti, Characterization of microalga Chlorella as a fuel and its thermogravimetric behavior, Appl. Energy 102 (2013) 24–31.
[42] D. López-González, M. Fernandez-Lopez, J.L. Valverde, L. Sanchez-Silva, Kinetic analysis and thermal characterization of the microalgae combustion process by thermal analysis coupled to mass spectrometry, Appl. Energy 114 (2014) 227–237.
[43] S. Sukarni, U. Yanuhar, I.N.G. Wardana, S. Sudjito, N. Hamidi, W. Wijayanti, Y. Wibisono, S. Sumarli, I.M. Nauri, H. Suryanto, Combustion of microalgae Nannochloropsis oculata biomass: cellular macromolecular and mineralogical content changes during thermal decomposition, Songklanakarin J. Sci. Technol. 40 (2018) 1456–1463.
[44] S. Ren, J. Zhang, Thermogravimetric analysis of anthracite and waste plastics by iso-conversional method, Thermochim, Acta 561 (2013) 36–40.
[45] P. Grammelis, P. Basinas, A. Malliopoulou, G. Sakellaropoulos, Pyrolysis kinetics and combustion characteristics of waste recovered fuels, Fuel 88 (2009) 195–205.
[46] Y.T. Tang, X.Q. Ma, Z.Y. Lai, Y. Fan, Thermogravimetric analyses of co-combustion of plastic, rubber, leather in N2/O2 and CO2/O2 atmospheres, Energy 90 (2015) 1066–1074.
[47] Y. Lin, X. Ma, X. Peng, Z. Yu, S. Fang, Y. Lin, Y. Fan, Combustion, pyrolysis and char CO2-gasification characteristics of hydrothermal carbonization solid fuel from municipal solid wastes, Fuel 181 (2016) 905–915.
[48] Sudjito Sukarni, N. Hamidi, U. Yanuhar, I.N.G. Wardana, Potential and properties of marine microalgae Nannochloropsis oculata as biomass fuel feedstock, Int. J. Energy Environ. Eng. 5 (2014) 279–290.
[49] X. Guo, Z. Wang, H. Li, H. Huang, C. Wu, Y. Chen, B. Li, A study on combustion characteristics and kinetic model of municipal solid wastes, Energy Fuel. 15 (2001) 1441–1446.
[50] A. Plis, J. Lasek, A. Skawińska, Kinetic analysis of the combustion process of Nannochloropsis gaditana microalgae based on thermogravimetric studies, J. Anal. Appl. Pyrolysis 127 (2017) 109–119.
[51] Y. Fan, Z. Yu, S. Fang, Y. Lin, Y. Lin, Y. Liao, X. Ma, Investigation on the co-combustion of oil shale and municipal solid waste by using thermogravimetric analysis, Energy Convers. Manag. 117 (2016) 367–374.
[52] K. Açikalin, Pyrolytic characteristics and kinetics of pistachio shell by thermogravimetric analysis, J. Therm. Anal. Calorim. 109 (2012) 227–235.
[53] R. López, C. Fernández, J. Cara, O. Martínez, M.E. Sánchez, Differences between combustion and oxy-combustion of corn and corn-rape blend using thermogravimetric analysis, Fuel Process. Technol. 128 (2014) 376–387.
[54] S. Pickard, S.S. Daood, M. Pourkashanian, W. Nimmo, Reactivity during bench-scale combustion of biomass fuels for carbon capture and storage applications, Fuel 134 (2014) 166–170.
[55] A. Anca-Couce, A. Berger, N. Zobel, How to determine consistent biomass pyrolysis kinetics in a parallel reaction scheme, Fuel 123 (2014) 230–240.
[56] M.V. Gil, D. Casal, C. Pevida, J.J. Pis, F. Rubiera, Thermal behaviour and kinetics of coal/biomass blends during co-combustion, Bioresour. Technol. 101 (2010) 5601–5608.
[57] S.Y. Yorulmaz, A.T. Atimtay, Investigation of combustion kinetics of treated and untreated waste wood samples with thermogravimetric analysis, Fuel Process. Technol. 90 (2009) 939–946.
[58] K. Açikalin, Thermogravimetric analysis of walnut shell as pyrolysis feedstock, J. Therm. Anal. Calorim. 105 (2011) 145–150.
[59] S. Sukarni, A. Prasetiyo, S. Sumarli, I.M. Nauri, A.A. Permanasari, Kinetic analysis of co-combustion of microalgae Spirulina platensis and synthetic waste through the fitting model, in: MATEC Web Conf., EDP Sciences, 2018, 00009.
[60] S. Sukarni, A.E. Widiono, S. Sumarli, R. Wulandari, I.M. Nauri, A.A. Permanasari, Thermal decomposition behavior of water hyacinth (Eichhornia crassipes) under an inert atmosphere, in: MATEC Web Conf., EDP Sciences, 2018, 00010.
[61] A. Jimenez, V. Berencuer, J. Lopez, A. Sanchez, Thermal degradation study of poly (vinyl chloride): kinetic analysis of thermogravimetric data, J. Appl. Polym. Sci. 50 (1993) 1565–1573.
[62] J. Zsako, Kinetic analysis of thermogravimetric data, VI - some problems of deriving kinetic parameters from TG curves, J. Therm. Anal. 5 (1973) 239–251.
[63] Y. Gao, A. Tahmasebi, J. Dou, J. Yu, Combustion characteristics and air pollutant formation during oxy-fuel co-combustion of microalgae and lignite, Bioresour. Technol. 207 (2016) 276–284.
[64] A.K. Galwey, M.E. Brown, Application of the arrhenius equation to solid state kinetics: can this be justified? Thermochim. Acta 386 (2002) 91–98.
[65] J.E. White, W.J. Catallo, B.L. Legendre, Biomass pyrolysis kinetics: a comparative critical review with relevant agricultural residue case studies, J. Anal. Appl. Pyrolysis 91 (2011) 1–33.
[66] A.J. Tsamba, W. Yang, W. Blasiak, Pyrolysis characteristics and global kinetics of coconut and cashew nut shells, Fuel Process. Technol. 87 (2006) 523–530.
[67] Z.S. Petrović, Z.Z. Zavargo, Reliability of methods for determination of kinetic parameters from thermogravimetry and DSC measurements, J. Appl. Polym. Sci. 32 (1986) 4353–4367.
[68] B. Fidalgo, M. Chilmeran, T. Somorin, A. Sowale, A. Kolios, A. Parker, L. Williams, M. Collins, E.J. McAdam, S. Tyrrel, Non-isothermal thermogravimetric kinetic analysis of the thermochemical conversion of human faeces, Renew. Energy 132 (2019) 1177–1184.
[69] A.W. Date, Analytic Combustion with Thermodynamics, Chemical Kinetics and Mass Transfer, Springer Singapore, 2020.
[70] M.E. Brown, A.K. Galwey, The significance of “compensation effects” appearing in data published in “computational aspects of kinetic analysis”: ICTAC project, Thermochim. Acta 387 (2002) (2000) 173–183.
[71] C. Wang, X. Zhang, Y. Liu, D. Che, Pyrolysis and combustion characteristics of coals in oxyfuel combustion, Appl. Energy 97 (2012) 264–273.
[72] S. Vyazovkin, Two types of uncertainty in the values of activation energy, J. Therm. Anal. Calorim. 64 (2001) 829–835.
[73] E. Sima-Ella, G. Yuan, T. Mays, A simple kinetic analysis to determine the intrinsic reactivity of coal chars, Fuel 84 (2005) 1920–1925.
[74] E. Chornet, C. Roy, Compensation effect in the thermal decomposition of cellulosic materials, Thermochim. Acta 35 (1980) 389–393.
[75] J.H. Flynn, The Arrhenius equation in condensed phase kinetics, J. Therm. Anal. 36 (1990) 1579–1593.
[76] N. Liu, B. Wang, W. Fan, Kinetic compensation effect in the thermal decomposition of biomass in air atmosphere, Fire Saf. Sci. (2003) 581–592.
[77] N. Koga, J. Šesták, Kinetic compensation effect as a mathematical consequence of the exponential rate constant, Thermochim. Acta 182 (1991) 201–208.
[78] X. Liu, M. Chen, Y. Wei, Kinetics based on two-stage scheme for co-combustion of herbaceous biomass and bituminous coal, Fuel 143 (2015) 577–585.
[79] N.A. Liu, W. Fan, R. Dobashi, L. Huang, Kinetic modeling of thermal decomposition of natural cellulosic materials in air atmosphere, J. Anal. Appl. Pyrolysis 63 (2002) 303–325.